Bioresource Technology 218 (2016) 351–359

Contents lists available at ScienceDirect

Bioresource Technology

journal homepage: www.elsevier.com/locate/biortech

Investigation of the adsorption-reduction mechanisms of hexavalent chromium by ramie biochars of different pyrolytic temperatures

Lu Zhou [a,b], Yunguo Liu [a,b,*], Shaobo Liu [c], Yicheng Yin [a,b], Guangming Zeng [a,b], Xiaofei Tan [a,b], Xi Hu [d], Xinjiang Hu [a,b], Luhua Jiang [a,b], Yang Ding [a,b], Shaoheng Liu [a,b], Xixian Huang [a,b]

[a] College of Environmental Science and Engineering, Hunan University, Changsha 410082, PR China
[b] Key Laboratory of Environmental Biology and Pollution Control (Hunan University), Ministry of Education, Changsha 410082, PR China
[c] College of Architecture and Art, Central South University, Changsha 410082, PR China
[d] College of Environmental Science and Engineering Research, Central South University of Forestry and Technology, Changsha 410004, PR China

HIGHLIGHTS

- Ramie residue can be converted into biochar as an effective sorbent for Cr(VI) removal.
- Cr(VI) sorption on the biochars was dependent on their physiochemical properties resulting from pyrolysis temperature.
- Both electrostatic and ionic interactions were responsible for Cr(VI) adsorption and reduction.
- The low-temperature biochar had better adsorption capability due to its abundant carboxyl and hydroxyl groups.

ARTICLE INFO

Article history:
Received 16 April 2016
Received in revised form 18 June 2016
Accepted 21 June 2016
Available online 27 June 2016

Keywords:
Ramie residues
Biochar
Pyrolysis temperature
Chromium
Mechanisms

ABSTRACT

To investigate the relationship between Cr(VI) adsorption mechanisms and physio-chemical properties of biochar, ramie residues were oxygen-limited pyrolyzed under temperature varying from 300 to 600 °C. Batch adsorption experiments indicated that higher pyrolysis temperature limits Cr(VI) sorption in terms of capacity and affinity due to a higher aromatic structure and fewer polar functional groups in biochar. Both electrostatic (physical) and ionic (chemical) interactions were involved in the Cr(VI) removal. For low-temperature biochar, the simple physical adsorption was limited and the significant improvement in Cr(VI) sorption was attributed to abundant carboxyl and hydroxyl groups. The adsorption-reduction mechanisms could be concluded that Cr(VI) ions were electrostatically attracted by the positively charged biochar surface and reduced to Cr(III), and then the converted Cr(III) was retained or discharged into the solution. The study demonstrates ramie residues can be converted into biochar as a low-cost and effective sorbent for Cr(VI) removal.

1. Introduction

Chromium (Cr), a common contaminant in surface water and groundwater, is mainly derived from industrial processes such as leather tannery, electroplating, mining, metallurgy, steel manufacturing, textile, etc (Bayazit and Kerkez, 2014). In general, Cr occurs in aqueous media as two major valence states, the trivalent [Cr(III)] and hexavalent [Cr(VI)] states. Cr(III) is an essential bioelement to mammals at low concentration and is rather immobile in natural environment. Cr(VI) is five hundred times more poisonous than Cr(III) and may cause carcinogenesis, mutation or teratogenesis to living creatures (Chen et al., 2015; Suksabye and Thiravetyan, 2012). Depending on the pH levels, Cr(VI) primarily exists in the form of chromate (CrO_4^{2-} and $HCrO_4^-$) and dichromate ($Cr_2O_7^{2-}$), which are highly toxic and water-soluble (Zelmanov and Semiat, 2011). Thus, Cr(VI) has been identified as a top-priority hazardous pollutant by the U.S. Environmental Protection Agency (EPA) (Ma et al., 2014). The Ministry of Environmental Protection in China has set the maximum permissible limit of Cr(VI) discharged in surface water to be below 0.05 mg L^{-1} according to the international standards (Zelmanov and Semiat, 2011). It is therefore of great significance to develop a cost-effective and reliable technique to eliminate Cr(VI) from industrial wastewater before being discharged into aquatic system. A variety of treatment technologies to remediate Cr(VI)-contaminated wastewater including chemical precipitation, membrane separation, oxidation/reduction, ion

* Corresponding author at: College of Environmental Science and Engineering, Hunan University, Changsha 410082, PR China.
E-mail address: liuyunguo_hnu@163.com (Y. Liu).

http://dx.doi.org/10.1016/j.biortech.2016.06.102
0960-8524/

exchange, adsorption, ultrafiltration and reverse osmosis have been proposed (Albadarin et al., 2012). Among them, adsorption process has evolved as the frontline for Cr(VI) disposal because of its high selectivity, economic efficiency and operation simplicity. However, the selection of low-cost and environmental-friendly adsorbent is a matter of concern (Albadarin et al., 2012; Chen et al., 2015).

Biochar, a carbon-rich product similar to activated carbon, is obtained by pyrolysis of biomass under relatively low temperature (<700 °C) and oxygen-limited environment (Tytlak et al., 2015). The conversion of waste biomass into biochar has received considerable interests due to its potential in soil amendment, crop fertilization, carbon sequestration and environmental remediation of heavy metals and organic pollutant (Chen et al., 2014; Tan et al., 2016). In comparison with activated carbon, the specific surface area and micropore volume of biochars are much smaller (Chen et al., 2014). However, the adsorption capacity of biochars in regard to hazardous cations and anions is comparable with that of activated carbon. Due to its abundant functional groups and lower cost, biochar is a best replacement of commercial activated carbon (Chen et al., 2015; Tytlak et al., 2015). Generally, there are different kinds of mechanisms for Cr(VI) removal by biochars: (i) electrostatic interaction, where Cr(VI) ions are adsorbed on the positively charged surface of sorbent without any Cr(VI) reduction; (ii) complete reduction, where Cr(VI) ions are adsorbed and entirely reduced by sorbent to Cr(III) form; (iii) cationic adsorption, where Cr(VI) ions are entirely reduced by sorbent to Cr(III) form and then adsorbed onto the sorbent; (iv) adsorption coupled with reduction, where Cr(VI) ions are partly adsorbed onto the sorbent and the remainder are reduced to Cr(III) form (Tytlak et al., 2015). These different mechanisms responsible for Cr(VI) sorption by biochar are probably attributed to the chemical composition and properties of biochar, which largely depend on the characteristics of feedstock source and the pyrolysis conditions. Among pyrolysis conditions, temperature plays a key role in the pyrolysis process of feedstock and it greatly influences the physiochemical properties of biochar as well as the toxic ions' fate in the biochar body (Chen et al., 2014). It is well known that the chemical compositions of biochar are oxygen-containing functional groups, carbon fractions with aromatic structure and mineral constituents, which are greatly controlled by the pyrolysis temperature (Wang et al., 2015). A number of researches have been reported to determine how pyrolysis temperature as a critical factor of structural transformation translates into the function of biochar as a soil amendment, nature fertilizer, carbon sequestration agent or environmental sorbent (Mendez et al., 2013; Uchimiya et al., 2011; Yuan et al., 2014). However, very limited studies have been performed to elaborate the relationship between Cr(VI) adsorption and biochar properties based on different pyrolysis temperature. Thus, probing the exact mechanisms underlying Cr(VI) sorption by biochars produced from various temperatures is indispensable.

Biochar can be generated from various raw materials such as wood materials, switch grass, agricultural residues (cereal straw, nutshells and rice hulls), chicken litter, dairy manure and sewage sludge (Ahmad et al., 2012). To our knowledge, there is few research to date on the preparation and characterization of biochar produced from ramie residue via different pyrolysis temperature. Ramie (*Boehmeria nivea*) is a crop that extensively grown in Asian countries such as China, Philippines, India and Thailand. The coat of ramie stem is used for textile industry, whereas the decorticated stem is normally treated as solid waste. In China, the annual production of ramie residue is estimated to be approximately 450,000 tons (Wang and Wang, 2013). Additionally, ramie is mainly composed of cellulose (68.6–76.2%) (Liu et al., 2008), which is a linear macromolecule formed by anhydroglucose. Byproducts of cellulose pyrolysis include unsaturated anhydrosugars, catechol, diols and other compounds those can act as reducing and chelating agents toward metal ions (Mohan et al., 2011). Therefore, it is environmentally and financially viable to regard ramie residue as a good feedstock to make biochar.

In this study, oxygen-limited pyrolysis was used to prepare a series of ramie biochars using a laboratory-scale reactor at 300–600 °C, and then their physio-chemical properties were characterized. The main aims of this study were to: (i) investigate the effect of pyrolysis temperature on the characteristics and chemical composition of ramie biochar; (ii) determine Cr(VI) adsorption properties on the ramie biochars; (iii) probe the relationship between Cr (VI) sorption mechanisms and the properties of ramie biochar by using various instrumental analysis.

2. Materials and methods

2.1. Chemicals

All chemicals including HCl, NaOH, H_2SO_4, HNO_3, H_3PO_4, CH_3COCH_3, $C_{13}H_{14}N_4O$, and $K_2Cr_2O_7$ were analytical reagent grades. A stock solution (1000 mg L^{-1}) of Cr(VI) was prepared by dissolving $K_2Cr_2O_7$ in ultrapure water (Milli-Q Millipore, conductivity of 18.25 MΩ cm^{-1}). The working solutions of desired Cr(VI) concentrations were prepared daily by appropriately diluting the stock solutions.

2.2. Biochar preparation

Ramie residues, mainly the decorticated stems of ramies, were supplied by the farms in Changsha City, Hunan Province, China. The samples were air-dried at room temperature and then smashed to pass through a 100 mesh sieve (0.147 mm). The ground ramies were pyrolyzed at 300, 450, and 600 °C under 50 mL min^{-1} nitrogen flow rate using a muffle furnace with tubular reactor. The furnace was programmed to heat with a rate of 5 °C min^{-1} until it reached at a specified temperature and maintained the temperature for 2 h. The resulting biochars were allowed to cool down under nitrogen flow. Then the biochars were washed with deionized water for several times, dried at 60 °C for 24 h and sieved to a size ⩽0.147 mm. The dried biochars were stored in an airtight desiccator prior to use and were abbreviated as RB300, RB450 and RB600 respectively, according to the pyrolysis temperature.

2.3. Biochar characterization

Biochar yield was calculated as the ratio of the weight of biochar samples to that of dried ramie biomass. The pH value of biochar samples was determined by mixing biochar to deionized water at a ratio of 1:10 (w/v). The zeta potential of biochar was determined by using Electroacoustic Spectrometer (ZEN3600 Zetasizer UK) at varying solution pH from 2.0 to 8.0. The elemental composition of biochar was performed by an elemental analyzer (Vario EL III, Elementar, Germany). The surface area, pore size and pore volume were measured by the N_2 adsorption-desorption isotherm at 77.3 K using a Micromeritics TriStar II 3020. The surface morphology of biochar was observed by Quanta FEG 250 environmental scanning electron microscopy (SEM). The surface functional groups of biochar involved in the Cr(VI) removal were determined by Fourier transform infrared spectrophotometer (FTIR) (Nicolet 5700 Spectrometer, USA).

2.4. Adsorption experiments

Batch adsorption experiments of Cr(VI) were performed in triplicate in 100 mL sealed conical flasks on a thermostat water-wash

shaker at 160 rpm. In each procedure, 100 mg of ramie biochar was added into 50 mL of Cr(VI) solution in desired concentration. The pH of the suspension was adjusted by HNO_3 or NaOH solution (0.1–1 mol L^{-1}).

The impact of pH on Cr(VI) sorption by ramie biochars were conducted by adjusting the initial pH from 2.0 to 8.0 while keeping Cr(VI) concentration at 100 mg L^{-1}. All the suspensions were shaken at 25 °C for 24 h. For kinetic experiment, the Cr(VI) solutions (100 mg L^{-1}) were shaken at pH 2.0 for different time interval (15, 30, 60, 120, 180, 360, 480, 600, 720, 1080, 1440, 2160, and 2880 min). Adsorption isotherms were carried out by maintaining the water bath at 25 °C, with varied initial Cr(VI) concentrations (20, 50, 80, 100, 200, 250, 400, 500, and 800 mg L^{-1}). All the suspensions were also shaken at pH 2.0 for 24 h.

The initial and residual Cr(VI) concentrations were determined by a UV–vis spectrophotometer (UV-754N shanghai, China) at wavelength of 540 nm using the 1.5-diphenylcarbazide method. The corresponding total Cr was measured by an atomic adsorption spectrophotometer (TAS-990F, Beijing Persee, China). The amount of Cr adsorbed onto ramie biochars was determined by the simple concentration difference method. The adsorption capacities and efficiency of ramie biochars towards to Cr(VI) or total Cr were calculated as follows:

$$Q_e = \frac{(C_0 - C_e) \times V}{M} \quad (1)$$

$$R(\%) = \frac{C_0 - C_e}{C_0} \times 100\% \quad (2)$$

where Q_e is the adsorption capacities of ramie biochars; C_0 and C_e are the initial and equilibrium concentration of Cr(VI) or total Cr in solution (mg L^{-1}), respectively; V is the solution volume (mL); M is the mass of the ramie biochar used and R (%) is the adsorption efficiency.

2.5. Adsorption mechanism studies

RB300 was chosen as a typical material to investigate the adsorption mechanism of Cr. The surface morphological structure and elemental composition of RB300 before and after Cr adsorption were characterized by SEM coupled with an energy-dispersive spectrometer (EDS) (AMETER, USA). The FTIR spectrum (Nicolet 5700 Spectrometer, USA) was used to determine the changes in functional group on the RB300 before and after Cr adsorption. The valence state of the Cr adsorbed onto RB300 was determined by an ESCALAB 250Xi X-ray Photoelectron Spectrometer (XPS) (Thermo Fisher, USA).

2.6. Statistical analysis

The experimental data were presented as average values of triplicate samples. The different significance between each group was analyzed by Duncan's multiple range tests, taking $P < 0.05$ as significantly different. The kinetics model and adsorption isotherms were fitted by Origin Pro 8.0 (Origin Lab, USA). The conformity between experimental data and model estimated value was presented by the adjusted coefficient determination (R^2_{adj}), which was calculated as (Pan et al., 2006):

$$R^2_{adj} = 1 - R^2 \frac{m - b}{m - 1} \quad (3)$$

where R^2 is the standard coefficient of determination, m is the number of data points and b is the number of fitting parameters.

3. Results and discussion

3.1. Biochar characterization

3.1.1. Biochar yield and pH

The properties of ramie biochars including yield rate, pH and elemental composition are summarized in Table S1. As the pyrolysis temperature rose from 300 to 600 °C, the yield rate of biochars decreased from 75.57 wt% to 50.74 wt%, which may due to the dehydration reaction and thermal degradation of volatiles into low molecular weight liquids and gases (Thangalazhy-Gopakumar et al., 2010). A similar result was observed by Song et al. (Song and Guo, 2012) and the yield rate of ramie biochar was higher than those of biochars obtained from pitch pine (Kim et al., 2012), poultry litter (Song and Guo, 2012) and *Miscanthus* (Mimmo et al., 2014) at the same pyrolysis temperature. The increasing trend in pH value of ramie biochars was consistent with previous reports as a result of acidic surface group such as —COOH and —OH releases and carbonates formation ($CaCO_3$ and $MgCO_3$) during pyrolysis (Mendez et al., 2013; Yuan et al., 2014).

3.1.2. Elemental analysis

With increasing temperature, the carbon content increased from 45.48 to 70.20%, which was consistent with that in pitch pine biochar (Table S1) (Kim et al., 2012). This observation indicated that the increasing pyrolysis temperature may result in the acceleration of carbonization in biochar (Chen et al., 2012). Meanwhile, the loss of hydrogen, oxygen, nitrogen and sulfur was recorded at higher pyrolysis temperature, which was attributed to the cleavage of weak bonds within the biochar structure (Demirbas, 2004).

A Van Krevelen plot was employed to deduce the structural transformation in the biochars as a function of pyrolysis temperature (Fig. S1). It showed a significant decrease in the molar ratios of H/C and O/C compared to the raw material as pyrolysis temperature increased (Fig. S1). The molar ratio of H/C, a carbonization degree parameter, was lower than 0.5 when pyrolysis temperature reached 600 °C, thus suggesting that the RB600 with strong carbonization and aromatic structure can exist stably and resist decomposition (Yuan et al., 2013). The molar ratio of O/C in the ramie biochars was higher than that in activated carbon and the biochars produced from other biomass such as *Miscanthus* (Kim et al., 2013) and sewage sludge (Yuan et al., 2015), which indicated that the biochars with higher polarity have better adsorptive ability for polar materials than activated carbon and other categories of biochar (Chun et al., 2004). The molar ratio of O/C, with the same tendency of H/C, tended to decrease with pyrolysis temperature, resulting from the removal of polar surface functional groups during pyrolysis. These changes of H/C and O/C ratios well fitted the characteristic line on the Van Krevelen diagram, which illustrated that dehydrative polycondensation and dehydrogenative polymerization occur in the biochar structure (Chen et al., 2014; Uchimiya et al., 2011). Among these biochar samples, the highest H/C and O/C ratios were found at 300 °C, suggesting that the RB300 has considerable quantities of organic materials and polar functional groups.

3.1.3. Surface characters and micro morphology

The pore structure parameters of ramie biochars obtained from different temperature are presented in Table S1. It has been reported that pyrolysis conditions such as temperature and holding time could impact the surface area of biochars, and the largest surface area was markedly observed at 500–900 °C (Uchimiya et al., 2011). As can be seen in Table S1, the BET surface area of RB600 was 5.14 m^2 g^{-1}, which was the maximum among the three biochars. The surface area of ramie biochar was considerably less

than those of the most commercial adsorbents such as activated carbon (Chen et al., 2014) and comparable to the biochar from rice and maize straw (Wang et al., 2013). The RB300 was characterized by the second largest surface area together with its maximum pore volume, which suggested that the RB300 could provide a higher level of contacting area and more adsorption sites for Cr(VI) removal. The average pore sizes of RB300, RB450 and RB600 were about 12.79, 14.31 and 12.50 nm, respectively. As shown in Fig. S2, pore structure in the biochars was mainly made up by the mesopores (pores diameter between 2 nm and 50 nm), which was consistent with the pore structure in other biochar from sewage sludge (Yuan et al., 2015) and swine manure (Tsai et al., 2012).

The morphological changes in the pore structure of ramie biochars are shown in a SEM micrograph (Fig. S3). It can be seen that the RB300 had a rough and complex surface containing pores with different sizes and shapes. As pyrolysis temperature increased, feedstock decomposition increased and the biochar especially RB600 revealed its underlying channel structure, which indicated that the structure of biochar was well carbonized at high pyrolysis temperature due to the removal of volatile matter such as cellulose and hemicellulose (Kim et al., 2012).

3.1.4. FTIR analysis

FTIR spectrums of the biochars produced at different temperatures are compared in Fig. S4. The surface functional groups of ramie biochars included —OH, —CH, C=O and CO—, which may be responsible for Cr removal. The broad peaks at about 3430 cm^{-1} and 1054 cm^{-1} were observed in the biochars, indicating the presence of O—H stretching vibration in hydroxyl groups and alcohol groups of glucose (C-OH) (Mendez et al., 2013; Yuan et al., 2015). Adsorption intensities at the band 2928 cm^{-1} and 1400 cm^{-1} were indicative of long linear aliphatic chain (—CH_2 and —CH_3) and decreased with the increasing pyrolysis temperature (Al-Wabel et al., 2013; Mimmo et al., 2014). The peaks at bands 1734 cm^{-1} and 1270 cm^{-1} were related to C=O stretching in carboxylic acid groups of hemicelluloses and aromatic CO— or phenolic —OH, which almost disappeared in the RB450 and RB600, suggesting the reduction of biochar surface polarity at the high pyrolysis temperature (Al-Wabel et al., 2013; Kim et al., 2013; Tytlak et al., 2015). The adsorption peak at 1615 cm^{-1}, which represented C=C stretching in the aromatic ring (Al-Wabel et al., 2013; Dong et al., 2013), became more pronounced as pyrolysis temperature increased. A new peak at 780 cm^{-1} for RB600 corresponding to aromatic C—H stretching was coincident with further condensation of biochar structure (Yuan et al., 2014). Thus, pyrolysis temperature had significant impact on the surface functional groups of biochars, resulting in the decrease of hydrophilic radicals and the development of aromatic structure, which was confirmed by the elemental analysis. Overall, the variation of biochar properties, tightly controlled by the pyrolysis temperature, would have huge impacts on their behavior of Cr(VI) adsorption.

3.2. Effect of pH on Cr(VI) adsorption

The initial pH is one of the most important parameters for the Cr(VI) removal, because it affects the surface charge of sorbent, the ionic state of functional groups on the sorbent surface as well as the form of chromium species in the adsorption system (Chen et al., 2015; Tytlak et al., 2015). The speciation of Cr(VI) in aqueous solution as a function of pH was simulated by Visual MINTEQ ver. 3.0 (Fig. 1). It could be found that $HCrO_4^-$ and $Cr_2O_7^{2-}$ were main ionic forms at pH 2.0–6.4, while CrO_4^{2-} was predominant in the range of pH > 6.4. The Cr(VI) sorption process was found to be pH dependent (Fig. 2), which indicated that the ramie biochars were more active under acidic conditions and maximum adsorption occurred at pH 2.0. There was a sharp decrease in the percentage

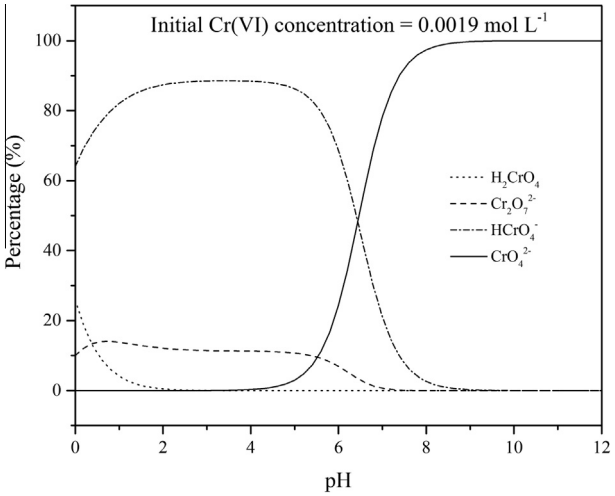

Fig. 1. The speciation diagram for Cr(VI) in aqueous solution as a function of pH, simulated by Visual MINTEQ ver. 3.0. pH ranges from 1 to 10 with the step length of 0.1. The initial Cr(VI) concentration was 0.0019 mol L^{-1}.

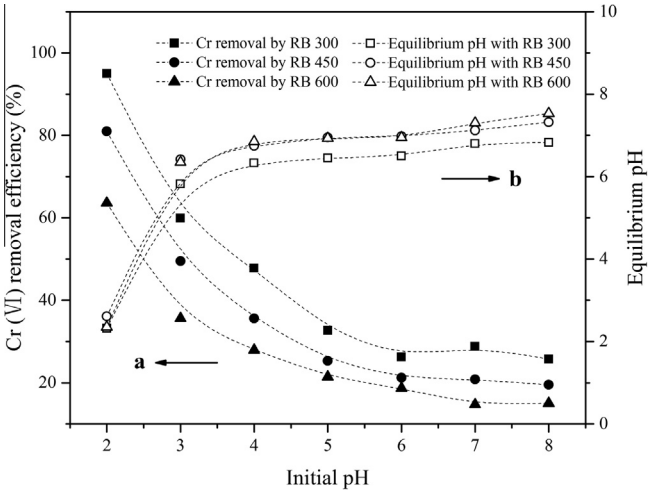

Fig. 2. (a) Effect of the initial pH on Cr(VI) removal using biochars produced at various temperatures. (b) Relationship between the initial and equilibrium pH of the sample solution (initial Cr(VI) concentration = 100 mg L^{-1}; sorbent dose = 2 g L^{-1}; contact time = 24 h).

of Cr(VI) removal when pH was raised from 2.0 to 8.0, which supported that the ion exchange and electronic interactions might be involved in the Cr(VI) adsorption mechanism (Albadarin et al., 2012). The zeta-potential-pH curves of ramie biochars before and after Cr(VI) removal were shown in Fig. S5. For pH < pH_{pzc} (point of zero charge), the hydroxyl groups were protonated and the biochar surface was positively charged, which would electrostatically attract the negatively charged chromate ions and increase its diffusion into the bulk of ramie biochar (Tan et al., 2015). In the same way, the decrease in the Cr(VI) removal at higher pH could be due to the electrostatic repulsion between the chromate ions and negatively charged biochar surface. As can be seen that the presence of Cr(VI) shifted the zeta-potential-pH curves of ramie biochars in a positive direction, and the difference in zeta potential between systems of biochar and biochar + Cr(VI) was specially pronounced at pH 2.0, which could be attributed to specific adsorption of the reduced Cr(III) (Tong et al., 2011). Arslan and Pehlivan (2007) reported that at low pH, Cr(III) is mainly present as Cr^{3+} and the carboxylic acid sites could be appreciably deprotonated (COO^-) to form chemical bonds with Cr^{3+}, thus affecting the surface charge

and surface potential of biochars. Meanwhile, the pH value elevated by a certain extent after the equilibrium is reached due to the buffering capacity of biochar, which may result from the release of alkaline substances in the biochar such as CaO and MgO (Chen et al., 2015). Hence, pH 2.0 was taken as the optimal value for the Cr(VI) removal by ramie biochar.

3.3. Comparative analysis

The comparison of Cr sorption characteristics by RB300, RB450 and RB600 were performed by varying time from 0.25 h to 48 h (Fig. 3). As seen, Cr(VI) removal by all ramie biochars exhibited initial high removal efficiency within first 12 h, and then reached the equilibrium in 48 h with a small variation. For example, Cr(VI) was rapidly sorbed onto RB300 within 12 h, which accounted for 82.95% to its total amount of adsorption. It is suggested that 24 h will be sufficient to reach the equilibrium state for Cr(VI) adsorption by ramie biochars in the following research. At the end of adsorption process, RB300, RB450 and RB600 removed about 99.10%, 82.00% and 63.60% of Cr(VI), with final adsorption capacity of 49.55 mg g^{-1}, 41.00 mg g^{-1} and 31.80 mg g^{-1}, respectively. Meanwhile, Cr(III) concentration increased in proportion to the Cr(VI) elimination, which indicated that the Cr(VI) adsorbed onto ramie biochars surface could be reduced to Cr(III). After 48 h, almost 22.80%, 25.12% and 23.82% of Cr(VI) was transferred to Cr (III) by RB300, RB450 and RB600, respectively, and then was released into the aqueous solution. In addition, a part of converted Cr(III) was still adsorbed by the biochar in the form of aqueous complex $[Cr(H_2O)_5]^{3+}$ (Tytlak et al., 2015). In comparison of the Cr(VI) removal efficiency and the release amount of Cr(III), RB300 is the best material for Cr(VI) adsorption.

3.4. Adsorption kinetics

In order to make validate the mechanism of Cr(VI) adsorption and its potential rate-controlling steps including mass transfer, intraparticle diffusion and chemical reaction processes, various kinetic models were applied to simulate the experimental data.

3.4.1. Pseudo-first-order and pseudo-second-order models

The pseudo-first-order (Eq. (4)) and pseudo-second-order (Eq. (5)) models are often used to fit the experimental data (Nityanandi and Subbhuraam, 2009):

$$\log(q_e - q_t) = \log q_e - \frac{k_1}{2.303}t \quad (4)$$

$$\frac{t}{q_t} = \frac{1}{k_2 q_e^2} + \frac{1}{q_e}t \quad (5)$$

where q_e and q_t (mg g^{-1}) are the adsorption capacities of biochars at equilibrium and time t, respectively, and k_1 (min^{-1}) and k_2 (g mg^{-1} min^{-1}) are the corresponding adsorption rate constant. The calculated results of first-order and second-order rate equations are shown in Table 1. The correlation coefficient (R^2_{adj}) suggested that the pseudo-second-order model (R^2_{adj} = 0.996–0.997) was better fitted with the experimental data compared to the pseudo-first-order model (R^2_{adj} = 0.928–0.939). Meanwhile, the adsorption capacity of calculated from pseudo-second-order equation was more consistent with the experimental q_e value. The plots of t/q_t versus t for pseudo-second-order equation are shown in Fig. 4a. Thus the experimental results supported the assumption behind the pseudo-second-order model that the mechanism of Cr(VI) adsorption was closer to chemisorption, which involved valency forces through sharing or exchanging electrons between the ramie biochars and Cr(VI) ions (Tytlak et al., 2015). The better correlation of kinetics data to the pseudo-second-order model was also reported in previous study used by various biochars (Ma et al., 2014; Tytlak et al., 2015).

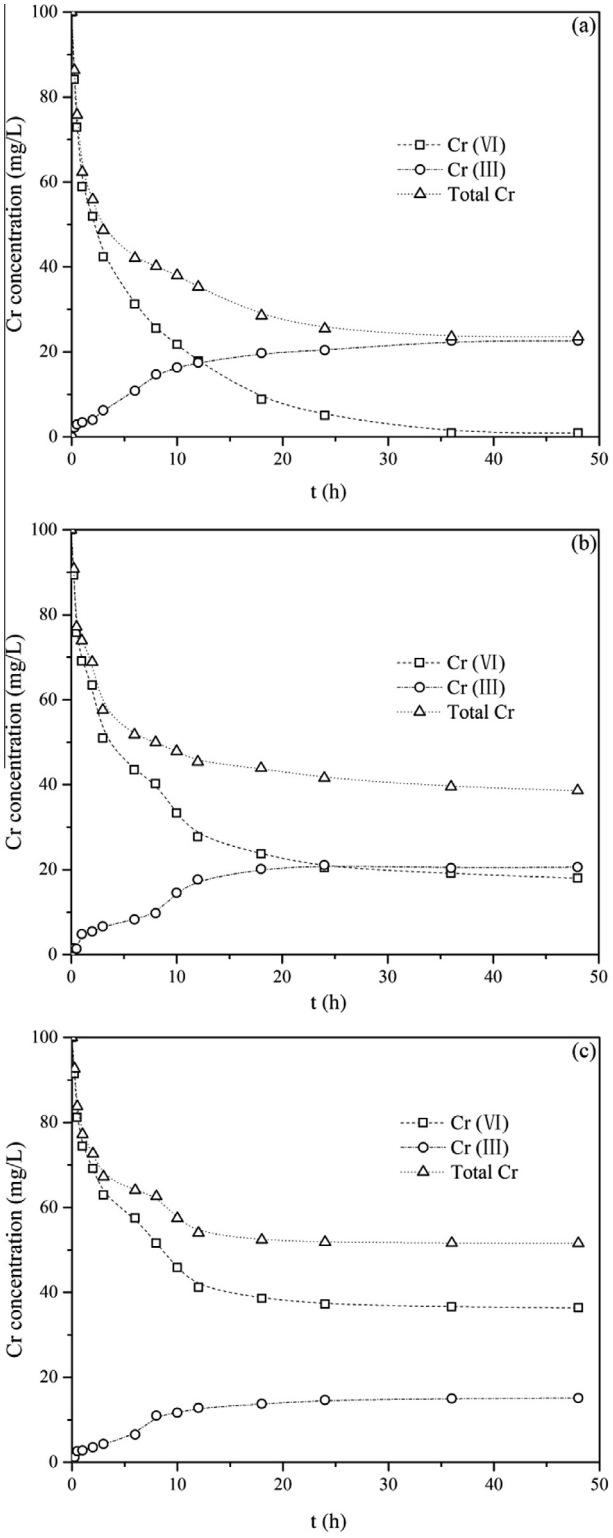

Fig. 3. The comparison of Cr(VI) removal by RB300 (a), RB450 (b) and RB600 (c) as a function of time (initial Cr(VI) concentration = 100 mg L^{-1}; sorbent dose = 2 g L^{-1}; pH = 2).

3.4.2. Two-compartment model

Furthermore, the time-courses of Cr(VI) sorption onto ramie biochars were analyzed with a two-compartment and first-order

Table 1
The fitting results of Cr(VI) sorption on ramie biochars using two-compartment (TC), pseudo-first-order and pseudo-second-order model.

Biochar	TC model					Pseudo-first-order model			Pseudo-second-order model		
	F_{fast}	F_{slow}	k_{fast}	k_{slow}	R^2_{adj}	Q_e	k_1	R^2_{adj}	Q_e	$k_2 \times 10^3$	R^2_{adj}
RB 300	0.601	0.399	9.550	0.546	0.999	44.47	0.381	0.928	51.33	0.161	0.996
RB 450	0.654	0.346	7.919	0.482	0.995	37.60	0.334	0.939	42.55	0.195	0.997
RB 600	0.674	0.326	7.334	0.442	0.995	29.82	0.334	0.938	33.11	0.276	0.997

dynamics model (TC model, Eq. (6)), which can be presented as follows (Pan et al., 2006):

$$\frac{q_t}{q_{t=\infty}} = F_{fast}(1 - e^{-t/k_{fast}}) + F_{slow}(1 - e^{-t/k_{slow}}) \quad (6)$$

where q_t (mg g^{-1}) and $q_{t=\infty}$ (mg g^{-1}) are the amounts of adsorbed Cr (VI) on the biochars at time t and equilibrium, respectively. Parameters of F_{fast} and F_{slow} are the mass fractions of "fast" and "slow" compartments, respectively, and $F_{fast} + F_{slow} = 1$. Parameters of k_{fast} (h^{-1}) and k_{slow} (h^{-1}) are the first-order rate constants for transfer into "fast" and "slow" compartments of the biochars by TC model.

Current kinetics model considered the adsorption of Cr(VI) by ramie biochars as a two-domain process, which could be divided into "fast" and "slow" compartments. As shown in Table 1, the TC model well fitted the dynamics data of Cr(VI) adsorption on RB300, RB450 and RB600 with R^2_{adj} ranged in 0.995–0.999. The F_{fast} value of RB300, RB450 and RB600 were much greater than those of F_{slow}, indicating that the fast sorption stage was predominant during Cr(VI) sorption process. As can be seen in Fig. 4b, during a relatively short contact time, such as 10 h, the fast compartment achieved 79.01%, 81.34% and 85.22% of their own sorption capacity of RB300, RB450 and RB600, respectively, while the sorption capacity contributed by slow compartment only reached about 20% between 10 h and 48 h. The k_{fast} value of Cr(VI) sorption declined with the increasing pyrolysis temperature, thus the reaction between Cr(VI) and the adsorption sites of biochar obtained at lower temperature was more active. It is commonly considered that the electrostatic interaction between Cr(VI) species and acidic oxygen-containing functional groups is responsible for the fast sorption of Cr(VI) and may reach equilibrium in a short period (Wang et al., 2015). Due to the reduction or even disappearance of those oxygen-containing functional groups in high-temperature biochar, the rate of fast adsorption was weakened along with the increasing pyrolysis temperature.

3.4.3. Intraparticle and film diffusion model

The kinetics data were tested against the intraparticle diffusion model and the film diffusion model of Boyd to identify the actual rate-controlling steps involved in the Cr(VI) sorption process. Generally, the sorption process of a sorbate by a porous sorbent can be classified as three steps as follows: (i) external mass transfer across the hydrodynamic boundary layer film surrounding the sorbent particle, (ii) intraparticle diffusion of the sorbate molecules within the sorbent pores either by liquid filled pores or a solid surface diffusion process, and (iii) adsorption at an active site on the external or internal surface of sorbent. The third step is often considered to be extremely rapid, thus the most contribution to the rate of adsorption are film or/and pore diffusion (Hu et al., 2011). The intraparticle diffusion model can be represented as follows (Hu et al., 2011):

$$q_t = k_p t^{1/2} + C \quad (7)$$

where k_p is the intraparticle diffusion rate constant (mg g^{-1} $h^{1/2}$), and C is the intercept (mg g^{-1}) and its value stand for the thickness of boundary layer. The longer the intercept length is, the more likely it is that Cr(VI) sorption is mainly controlled by boundary layer. The plots of q_t versus $t^{1/2}$ are shown in Fig. 4c and the k_p for the sorption of Cr(VI) onto ramie biochars is represented as the slope of the plot. The intraparticle diffusion coefficients for RB300, RB450 and RB600 were 6.99, 5.90 and 4.62 mg g^{-1} $h^{1/2}$, respectively. The intercept values decreased with the increasing pyrolysis temperature, indicating that the boundary layer had the most obvious impact on RB300 (Al-Othman et al., 2012). The multi-linear plot confirmed that the Cr(VI) ions transfer was a multi-step process, which behaved as mainly three linear regions in the plot, implying that the intraparticle diffusion was not the rate-controlling step for the overall reaction. The calculated intercept values suggested that the Cr(VI) sorption proceeded from mass transfer across the interface of boundary layer to the intraparticle diffusion within the pores of sorbent (Albadarin et al., 2012). In order to determine whether the actual rate-controlling step results from film diffusion or pore diffusion, the kinetic data have been analyzed using the Boyd model, which is given as (Hu et al., 2011):

$$F = 1 - \frac{6}{\pi^2}\sum_{m=1}^{\infty}\frac{1}{m^2}\exp\left[\frac{-D_i\pi^2 m^2 t}{r^2}\right] \quad (8)$$

or

$$F = 1 - \frac{6}{\pi^2}\sum_{m=1}^{\infty}\frac{1}{m^2}\exp(-m^2 B_t) \quad (9)$$

where F is the fractional achievement of equilibrium at time t and it can be calculated by the following equation:

$$F = \frac{q_t}{q_e} \quad (10)$$

Thus, the kinetic expression can be simplified as:

$$B_t = -0.4977 - \ln(1 - F) \quad (11)$$

The value of B_t can be calculated for each q_e value, and then plotted against t to form the so-called Boyd plots. If the Boyd plot is a straight line passing through the origin, the rate-limiting processes of Cr(VI) sorption are governed by pore-diffusion mechanism; otherwise they are mainly controlled by film diffusion (Albadarin et al., 2012; Hu et al., 2011). The plots of RB300, RB450 and RB600 neither illustrated the linearity over the period nor passed through the origin (Fig. S6), indicating that the external mass transfer was the initial rate-limiting process in the Cr(VI) sorption system. Similar results were observed in the Cr(VI) sorption onto dolomite absorbent (Albadarin et al., 2012). It has been reported that the mass transfer mechanisms are affected by a number of factors such as shaking speed, particle size of sorbent, sorbate concentration or the affinity between sorbent and sorbate. Usually, the rate-limiting step controlled by film diffusion is indicative of the poor mixing, small particle size, dilute concentration of sorbent and high affinity between sorbent and sorbate in the systems. On the contrary, the pore diffusion limits the overall rate of mass transfer in the systems which have been well stirred, large particle size, high concentration of sorbent and low traction of sorbate for sorbent (Hu et al., 2011). In our study, both film and pore diffusions were simultaneously running during the Cr (VI) sorption process. However, the strong external resistance which was derived from the lower degree of agitation (160 rpm),

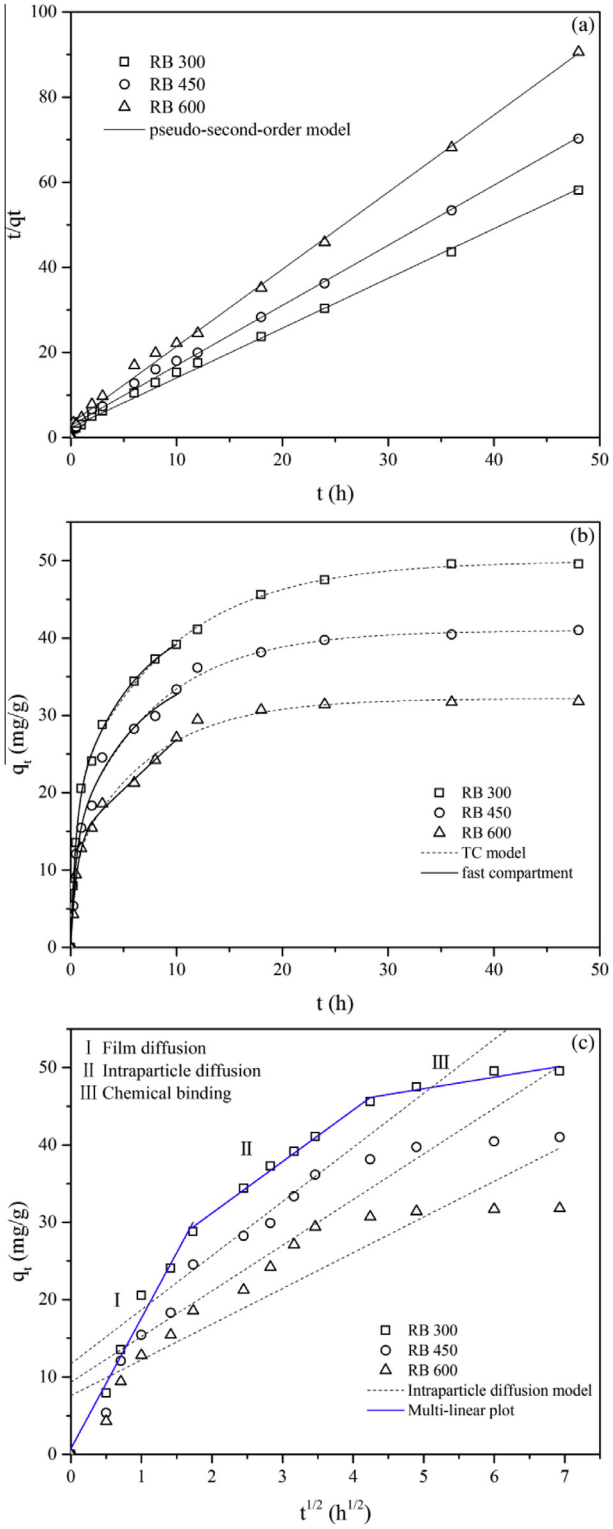

Fig. 4. Kinetics of Cr(VI) sorption onto biochars produced at various temperatures by fitting pseudo-second-order model (a), two-compartment (TC) model (b) and intraparticle diffusion model (c), respectively (initial Cr(VI) concentration = 100 mg L^{-1}; sorbent dose = 2 g L^{-1}; pH = 2).

low concentration of Cr(VI) (initial concentration of 100 mg L^{-1}) and small particle sizes of ramie biochars (below 147 μm) hindered the external mass transport. Meanwhile, the high affinity of Cr(VI) ions for ramie biochars effectively alleviated the internal resistance in the system, thus the rate-limiting step mainly governed by the film diffusion.

3.5. Adsorption isotherms

Batch experiments were carried out by varying the concentration of Cr(VI) from 20 to 800 mg L^{-1} to study adsorption isotherms, further explaining the adsorption mechanism of Cr(VI) ions onto biochar surfaces. Two typical isotherm models (Langmuir and Freundlich models) were applied to simulate the isothermal adsorption data. The Langmuir isotherm represents a system which the adsorption takes place on a monolayer surface without any interaction between adsorbed ions. It suggests that all adsorption sites are homogenously distributed on the biochar surface and once a metal ion occupied a site, no further adsorption would occur at that site (Deng et al., 2009). The empirical non-linear equations can be written as follows (Albadarin et al., 2012):

$$q_e = \frac{K_L q_{max} C_e}{1 + K_L C_e} \tag{12}$$

$$R_L = \frac{1}{1 + K_L C_0} \tag{13}$$

where q_{max} (mg g^{-1}) is the maximum adsorption capacity corresponding to complete monolayer coverage, q_e (mg g^{-1}) and C_e (mg L^{-1}) are the amount of adsorbed Cr(VI) and Cr(VI) concentration in the solution at equilibrium, respectively, C_0 (mg L^{-1}) is the lowest initial concentration of Cr(VI) in the solution, and K_L (L mg^{-1}) is the Langmuir constant related to binding energy. The R_L parameter is the dimensionless separation factor which indicates the shape of the Langmuir isotherm. The Freundlich model is another form of Langmuir approach for adsorption onto amorphous sorbent (Wong et al., 2004). It assumes that the non-ideal adsorption occurs on a heterogeneous surface accompanied by the presence of diverse functional groups and various interactions between sorbate and sorbent (Deng et al., 2009). The non-linear model can be expressed by the following equation (Albadarin et al., 2012):

$$q_e = K_F C_e^n \tag{14}$$

where K_F ((mg g^{-1}) (mg L^{-1})$^{-n}$) is the Freundlich constant related to adsorption capacity and n is an indicator of the adsorption intensity.

The sorption isotherms of Cr(VI) onto RB300, RB450 and RB600 are presented in Fig. 5 and the relevant parameters calculated from these models are listed in Table 2. As can be seen, the average value of R_L of Langmuir isotherm was between 0 and 1, indicating the favorable process of Cr(VI) onto the ramie biochar. For Freundlich

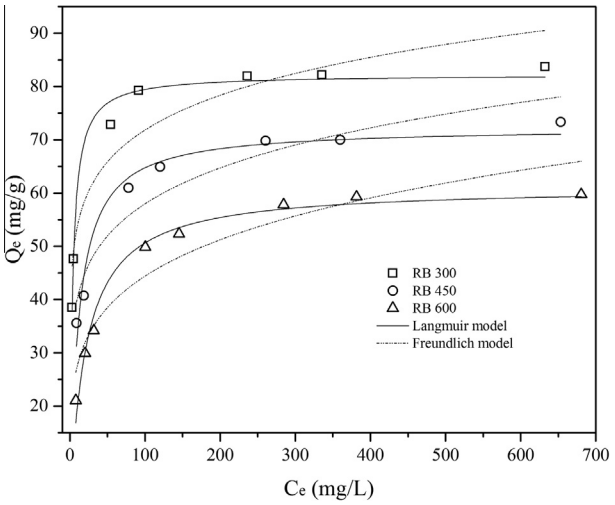

Fig. 5. Adsorption isotherms of Cr(VI) of biochars produced at various temperatures (initial Cr(VI) concentration = 20–800 mg L^{-1}; sorbent dose = 2 g L^{-1}; pH = 2; contact time = 24 h).

Table 2
Langmuir and Freundlich isotherms (LM and FM) constants for Cr(VI) sorption on ramie biochars.

Biochar	LM						FM					
	Q_m (mg g^{-1})	K_L (L mg^{-1})	R^2_{adj}	K_d (L g^{-1})			K_F (mg g^{-1}) (mg $L^{-1})^{-n}$	n	R^2_{adj}	K_d (L g^{-1})		
				10	200	500				10	200	500
RB 300	82.23	0.286	0.985	6.09	0.40	0.16	40.30	0.126	0.871	5.39	0.39	0.18
RB 450	72.32	0.085	0.964	3.32	0.34	0.14	27.95	0.158	0.901	4.02	0.32	0.15
RB 600	61.18	0.048	0.978	1.98	0.28	0.12	17.18	0.206	0.906	2.76	0.26	0.12

isotherm, all nonlinearity *n* values were less than 1 and the lower *n* values were obtained from the low-temperature biochars, which suggested that Cr(VI) sorption onto the ramie biochars had a great heterogeneity of sorption affinity and RB300 was more heterogeneous than the others (Wang et al., 2015). The experimental data were better fitted using Langmuir model with R^2_{adj} ranged between 0.964 and 0.988, implying that the monolayer coverage played a dominant role in the adsorption mechanism. Meanwhile, the maximum adsorption capacities based on Langmuir isotherm for RB300, RB450 and RB600 were calculated to be 82.23 mg g^{-1}, 72.31 mg g^{-1} and 61.18 mg g^{-1} respectively, which could be larger than those of other low-cost sorbents reported in the literature (Table S2).

Furthermore, the sorption coefficient K_d ($K_d = Q_e/C_e$, L g^{-1}) were calculated to evaluate their sorption capacities at different Cr(VI) equilibrium concentration (10, 200 and 500 mg L^{-1}) (Wang et al., 2015). As shown in Table 2, the K_d values for RB300, RB450 and RB600 greatly decreased with increasing Cr(VI) concentration, because Cr(VI) sorption on the ramie biochars was nonlinear. Regardless of Cr(VI) concentrations, all K_d values of RB300, calculated using Langmuir or Freundlich model, were greater than those of RB450 and RB600, indicating that RB300 had the strongest sorption affinity for Cr(VI) ions once more. The reduction of Cr(VI) sorption affinity on the high-temperature ramie biochar was possibly due to the markedly changed morphology, aromatic structure and content of functional groups in biochar, which could be supported by previous experimental data.

3.6. Mechanisms underlying Cr(VI) adsorption

From the above, it points out that the mechanism of adsorption included electrostatic (physical) interactions through film and intraparticle diffusions and ionic (chemical) interactions between Cr ions and the surface functional groups of ramie biochar. Given that the boundary layer has the most hindrance effect on RB300 and the surface area of RB300 is much smaller, the simple physical adsorption was limited in RB300, and the significant improvement in Cr(VI) adsorption was probably related to chemical interaction on the surface of RB300. To gain further insights into the mechanisms underlying Cr(VI) sorption on the ramie biochar, SEM-EDS, FTIR, and XPS techniques were used to analyze the exhausted RB300. The surface characteristic of RB300 based on SEM-EDS after reaction with Cr(VI) is shown in Fig. S7. The EDS spectra indicated the substantial amounts of K, Mg, Ca and Si in the RB300 and the accumulation of Cr on the RB300 after reaction with 100 mg L^{-1} Cr(VI). The FTIR spectrum of RB300 also underwent several changes after Cr(VI) sorption (Fig. S8). The disappearance of C=O stretching band at 1734 cm^{-1} was noted in Cr-loaded RB300, which indicated the involvement of carboxyl group in Cr(VI) sorption. Further, the peak intensity at 1270 cm^{-1} also decreased, typical of interaction of phenolic hydroxyl group with Cr ions. The results were in consistent with previous studies those which concluded that carboxyl and hydroxyl groups in the biochar are primarily responsible for sorption of heavy metal (Dong et al., 2011, 2013). Moreover, X-ray photoelectron spectroscopy was used to investigate the distribution of element species loaded onto RB300, then confirming the precise adsorption mechanism of Cr (VI) ions. The Cr2p spectra before and after Cr(VI) interaction are shown in Fig. S9 and the $Cr2p_{3/2}$ orbitals at binding energies of 577.0–580.0 eV are usually studied to identify the valence state of Cr (Tytlak et al., 2015). After Cr(VI) adsorption, the binding energies at 577.2 and 579.2 eV could be assigned to Cr(III) and Cr(VI), which accounted for 93.33% and 6.67%, respectively. The results suggested that both Cr(III) and Cr(VI) coexisted on the surface of Cr-loaded RB300 and most of the Cr bound to RB300 was Cr(III). In consideration of the detection of both Cr(III) and Cr(VI) in the aqueous solution, Cr(VI) removal mechanisms by ramie biochar could be divided into two processes: (i) direct adsorption by the positively charged ramie biochar, and reduction to Cr(III) when in contact with ramie biochar; (ii) and then a portion of the converted Cr(III) was retained by ramie biochar because of the complexation between Cr(III) ions and the functional groups and the remainder Cr(III) was discharged into the solution.

4. Conclusions

Cr(VI) sorption on ramie biochars was dependent on their structural, elemental and morphological properties resulting from pyrolysis temperature. Increasing pyrolysis temperature resulted in the decrease in Cr(VI) removal by the biochar. Both electrostatic interactions through film and intraparticle diffusions and chemical binding by polar functional groups were responsible for Cr(VI) adsorption and reduction. Based on the data, RB300 exhibited a strongest affinity for Cr(VI) ions mainly attributing to chemical interaction between Cr(VI) and carboxyl and hydroxyl groups. Thus, the low-temperature ramie biochar could serve as a potential alternative for remediation of Cr(VI) contaminated aqueous solution.

Acknowledgements

This work was funded by the National Natural Science Foundation of China (Grant No. 41271332) and the Natural Science Foundation of Guangdong Province, China (Grants No. 2016A030310246).

Appendix A. Supplementary data

Supplementary data associated with this article can be found, in the online version, at http://dx.doi.org/10.1016/j.biortech.2016.06.102.

References

Ahmad, M., Lee, S.S., Dou, X., Mohan, D., Sung, J.K., Yang, J.E., Ok, Y.S., 2012. Effects of pyrolysis temperature on soybean stover- and peanut shell-derived biochar properties and TCE adsorption in water. Bioresour. Technol. 118, 536–544.
Al-Othman, Z.A., Ali, R., Naushad, M., 2012. Hexavalent chromium removal from aqueous medium by activated carbon prepared from peanut shell: adsorption kinetics, equilibrium and thermodynamic studies. Chem. Eng. J. 184, 238–247.
Al-Wabel, M.I., Al-Omran, A., El-Naggar, A.H., Nadeem, M., Usman, A.R., 2013. Pyrolysis temperature induced changes in characteristics and chemical

composition of biochar produced from conocarpus wastes. Bioresour. Technol. 131, 374–379.
Albadarin, A.B., Mangwandi, C., Ala'a, H., Walker, G.M., Allen, S.J., Ahmad, M.N., 2012. Kinetic and thermodynamics of chromium ions adsorption onto low-cost dolomite adsorbent. Chem. Eng. J. 179, 193–202.
Arslan, G., Pehlivan, E., 2007. Batch removal of chromium(VI) from aqueous solution by Turkish brown coals. Bioresour. Technol. 98, 2836–2845.
Bayazit, Ş.S., Kerkez, Ö., 2014. Hexavalent chromium adsorption on superparamagnetic multi-wall carbon nanotubes and activated carbon composites. Chem. Eng. Res. Des. 92, 2725–2733.
Chen, T., Zhang, Y., Wang, H., Lu, W., Zhou, Z., Zhang, Y., Ren, L., 2014. Influence of pyrolysis temperature on characteristics and heavy metal adsorptive performance of biochar derived from municipal sewage sludge. Bioresour. Technol. 164, 47–54.
Chen, T., Zhou, Z., Xu, S., Wang, H., Lu, W., 2015. Adsorption behavior comparison of trivalent and hexavalent chromium on biochar derived from municipal sludge. Bioresour. Technol. 190, 388–394.
Chen, Y., Yang, H., Wang, X., Zhang, S., Chen, H., 2012. Biomass-based pyrolytic polygeneration system on cotton stalk pyrolysis: influence of temperature. Bioresour. Technol. 107, 411–418.
Chun, Y., Sheng, G., Chiou, C.T., Xing, B., 2004. Compositions and sorptive properties of crop residue-derived chars. Environ. Sci. Technol. 38, 4649–4655.
Demirbas, A., 2004. Effects of temperature and particle size on bio-char yield from pyrolysis of agricultural residues. J. Anal. Appl. Pyrol. 72, 243–248.
Deng, H., Yang, L., Tao, G., Dai, J., 2009. Preparation and characterization of activated carbon from cotton stalk by microwave assisted chemical activation—application in methylene blue adsorption from aqueous solution. J. Hazard. Mater. 166, 1514–1521.
Dong, X., Ma, L.Q., Li, Y., 2011. Characteristics and mechanisms of hexavalent chromium removal by biochar from sugar beet tailing. J. Hazard. Mater. 190, 909–915.
Dong, X., Ma, L.Q., Zhu, Y., Li, Y., Gu, B., 2013. Mechanistic investigation of mercury sorption by Brazilian pepper biochars of different pyrolytic temperatures based on X-ray photoelectron spectroscopy and flow calorimetry. Environ. Sci. Technol. 47, 12156–12164.
Hu, X.J., Wang, J.S., Liu, Y.G., Li, X., Zeng, G.M., Bao, Z.L., Zeng, X.X., Chen, A.W., Long, F., 2011. Adsorption of chromium (VI) by ethylenediamine-modified cross-linked magnetic chitosan resin: isotherms, kinetics and thermodynamics. J. Hazard. Mater. 185, 306–314.
Kim, K.H., Kim, J.Y., Cho, T.S., Choi, J.W., 2012. Influence of pyrolysis temperature on physicochemical properties of biochar obtained from the fast pyrolysis of pitch pine (*Pinus rigida*). Bioresour. Technol. 118, 158–162.
Kim, W.K., Shim, T., Kim, Y.S., Hyun, S., Ryu, C., Park, Y.K., Jung, J., 2013. Characterization of cadmium removal from aqueous solution by biochar produced from a giant Miscanthus at different pyrolytic temperatures. Bioresour. Technol. 138, 266–270.
Liu, Z.T., Yang, Y., Zhang, L., Sun, P., Liu, Z.W., Lu, J., Xiong, H., Peng, Y., Tang, S., 2008. Study on the performance of ramie fiber modified with ethylenediamine. Carbohydr. Polym. 71, 18–25.
Ma, Y., Liu, W.J., Zhang, N., Li, Y.S., Jiang, H., Sheng, G.P., 2014. Polyethylenimine modified biochar adsorbent for hexavalent chromium removal from the aqueous solution. Bioresour. Technol. 169, 403–408.
Mendez, A., Tarquis, A.M., Saa-Requejo, A., Guerrero, F., Gasco, G., 2013. Influence of pyrolysis temperature on composted sewage sludge biochar priming effect in a loamy soil. Chemosphere 93, 668–676.
Mimmo, T., Panzacchi, P., Baratieri, M., Davies, C.A., Tonon, G., 2014. Effect of pyrolysis temperature on miscanthus (*Miscanthus* × *giganteus*) biochar physical, chemical and functional properties. Biomass Bioenergy 62, 149–157.
Mohan, D., Rajput, S., Singh, V.K., Steele, P.H., Pittman Jr., C.U., 2011. Modeling and evaluation of chromium remediation from water using low cost bio-char, a green adsorbent. J. Hazard. Mater. 188, 319–333.
Nityanandi, D., Subbhuraam, C.V., 2009. Kinetics and thermodynamic of adsorption of chromium(VI) from aqueous solution using puresorbe. J. Hazard. Mater. 170, 876–882.
Pan, B., Xing, B., Liu, W., Tao, S., Lin, X., Zhang, Y., Yuan, H., Dai, H., Zhang, X., Xiao, Y., 2006. Two-compartment sorption of phenanthrene on eight soils with various organic carbon contents. J. Environ. Sci. Health B 41, 1333–1347.
Song, W., Guo, M., 2012. Quality variations of poultry litter biochar generated at different pyrolysis temperatures. J. Anal. Appl. Pyrol. 94, 138–145.
Suksabye, P., Thiravetyan, P., 2012. Cr(VI) adsorption from electroplating plating wastewater by chemically modified coir pith. J. Environ. Manage. 102, 1–8.
Tan, X., Liu, Y., Gu, Y., Xu, Y., Zeng, G., Hu, X., Liu, S., Wang, X., Liu, S., Li, J., 2016. Biochar-based nano-composites for the decontamination of wastewater: a review. Bioresour. Technol. 212, 318–333.
Tan, X., Liu, Y., Zeng, G., Wang, X., Hu, X., Gu, Y., Yang, Z., 2015. Application of biochar for the removal of pollutants from aqueous solutions. Chemosphere 125, 70–85.
Thangalazhy-Gopakumar, S., Adhikari, S., Ravindran, H., Gupta, R.B., Fasina, O., Tu, M., Fernando, S.D., 2010. Physiochemical properties of bio-oil produced at various temperatures from pine wood using an auger reactor. Bioresour. Technol. 101, 8389–8395.
Tong, X.J., Li, J.Y., Yuan, J.H., Xu, R.K., 2011. Adsorption of Cu(II) by biochars generated from three crop straws. Chem. Eng. J. 172, 828–834.
Tsai, W.T., Liu, S.C., Chen, H.R., Chang, Y.M., Tsai, Y.L., 2012. Textural and chemical properties of swine-manure-derived biochar pertinent to its potential use as a soil amendment. Chemosphere 89, 198–203.
Tytlak, A., Oleszczuk, P., Dobrowolski, R., 2015. Sorption and desorption of Cr(VI) ions from water by biochars in different environmental conditions. Environ. Sci. Pollut. Res. Int. 22, 5985–5994.
Uchimiya, M., Wartelle, L.H., Klasson, K.T., Fortier, C.A., Lima, I.M., 2011. Influence of pyrolysis temperature on biochar property and function as a heavy metal sorbent in soil. J. Agric. Food Chem. 59, 2501–2510.
Wang, B., Wang, K., 2013. Removal of copper from acid wastewater of bioleaching by adsorption onto ramie residue and uptake by *Trichoderma viride*. Bioresour. Technol. 136, 244–250.
Wang, Y., Hu, Y., Zhao, X., Wang, S., Xing, G., 2013. Comparisons of biochar properties from wood material and crop residues at different temperatures and residence times. Energy Fuels 27, 5890–5899.
Wang, Z., Liu, G., Zheng, H., Li, F., Ngo, H.H., Guo, W., Liu, C., Chen, L., Xing, B., 2015. Investigating the mechanisms of biochar's removal of lead from solution. Bioresour. Technol. 177, 308–317.
Wong, Y.C., Szeto, Y.S., Cheung, W.H., McKay, G., 2004. Adsorption of acid dyes on chitosan—equilibrium isotherm analyses. Process Biochem. 39, 695–704.
Yuan, H., Lu, T., Huang, H., Zhao, D., Kobayashi, N., Chen, Y., 2015. Influence of pyrolysis temperature on physical and chemical properties of biochar made from sewage sludge. J. Anal. Appl. Pyrol. 112, 284–289.
Yuan, H., Lu, T., Wang, Y., Huang, H., Chen, Y., 2014. Influence of pyrolysis temperature and holding time on properties of biochar derived from medicinal herb (*Radix isatidis*) residue and its effect on soil CO_2 emission. J. Anal. Appl. Pyrol. 110, 277–284.
Yuan, H., Lu, T., Zhao, D., Huang, H., Noriyuki, K., Chen, Y., 2013. Influence of temperature on product distribution and biochar properties by municipal sludge pyrolysis. J. Mater. Cycl. Waste Manage. 15, 357–361.
Zelmanov, G., Semiat, R., 2011. Iron (Fe^{+3}) oxide/hydroxide nanoparticles-based agglomerates suspension as adsorbent for chromium (Cr^{+6}) removal from water and recovery. Sep. Purif. Technol. 80, 330–337.